

Equilibrium line altitudes along the Andes during the Last millennium: Paleoclimatic implications

The Holocene
2017, Vol. 27(7) 1019–1033
© The Author(s) 2016
Reprints and permissions:
sagepub.co.uk/journalsPermissions.nav
DOI: 10.1177/0959683616678458
journals.sagepub.com/home/hol


Esteban A Sagredo,^{1,2} Thomas V Lowell,² Meredith A Kelly,³
Summer Rupper,⁴ Juan Carlos Aravena,⁵ Dylan J Ward² and
Andrew GO Malone⁶

Abstract

Deciphering the climate changes that influenced the glacial fluctuations of the last millennium requires documenting the spatial and temporal patterns of these glacial events. Here, we estimate the change in equilibrium line altitudes (ELAs) between the most prominent glacial advance of the last millennium and the present for four alpine glaciers located in different climatic regimes along the Andes. For each glacier, we reconstruct scenarios of climatic conditions (temperature and precipitation anomalies) that accommodate the observed ELA changes. We focus on the following glaciers: an alpine glacier in the Cordillera Vilcanota (13°S), Tapado glacier (30°S), Cipreses glacier (34°S), and Tranquilo glacier (47°S). Our results show that the range of possible temperature and precipitation anomalies that accommodate the observed ELA changes overlap significantly at three of the four sites (i.e. Vilcanota, Cipreses, and Tranquilo). Only Tapado glacier exhibits a set of climate anomalies that differs from the other three sites. Assuming no change in precipitation, the estimated ELA changes require a cooling of at least 0.7°C in the Cordillera Vilcanota, 1.0°C at Tapado glacier, 0.6°C at Cipreses glacier, and 0.7°C at Tranquilo glacier. Conversely, assuming no change in temperature, the estimated ELA changes are explained by increases in precipitation exceeding 0.52 m yr⁻¹ (64% of the annual precipitation) in the Cordillera Vilcanota, 0.31 m yr⁻¹ (89%) at Tapado glacier, 0.22 m yr⁻¹ (27%) at Cipreses glacier, and 0.3 m yr⁻¹ (27%) at Tranquilo glacier. By mapping the ELA changes and modeling the potential climate forcing across diverse climate settings, we aim to contribute toward documenting the spatial variability of climate conditions during the last millennium, a key step to decipher the mechanisms underlying the glacial fluctuation that occurred during this period.

Keywords

Andes, equilibrium line altitude, glacial fluctuations, glacial reconstruction, Holocene, last millennium

Received 28 February 2015; revised manuscript accepted 15 October 2016

Introduction

It has been recognized that during the last millennium, glaciers worldwide experienced major advances (e.g. Grove, 2004; Porter and Denton, 1967). Although, in both hemispheres, these glacial fluctuations broadly coincide with the European ‘Little Ice Age’ (AD 1850–1250) (Osborn and Briffa, 2006), at a centennial/decadal time scale, the inter-hemispheric synchrony of these glacial events is still under debate (Solomina et al., 2016). Thus, despite significant research efforts, the pattern, timing, and cause of these glacial fluctuations still remain elusive. Among the predominant hypotheses to explain the climatic changes underlying these glacial events are (1) reduction of solar irradiance (e.g. Denton and Karlén, 1973), (2) volcanism (e.g. Miller et al., 2012), (3) reorganization of the ocean circulation systems (e.g. Broecker, 2000), (4) large-scale climate internal variability (e.g. Moreno et al., 2014), or (5) some combination of the above. A comprehensive understanding of the spatial pattern of climate change during the last millennium is a key step for examining these hypotheses.

A multi-proxy global reconstruction of climate shows that the temperatures between CE 1400 and 1700 (the coldest period during the last millennium) exhibit a significant spatial variability (Mann et al., 2009). In this climate reconstruction, as in many others, the Southern Hemisphere is still underrepresented.

Paleoclimatic archives from South America (e.g. Boninsegna et al., 2009; Christie et al., 2011; Le Quesne et al., 2009; Masiokas et al., 2006; Morales et al., 2011; Moy et al., 2009; Villalba, 1994) are being integrated into preliminary reconstructions (Neukom et al., 2010, 2011). However, existing proxy records are spatially restricted, especially at high elevations.

Glacier systems offer one way to expand the network of proxy records of the last millennium climate in the Southern Hemisphere since they are distributed along the entire Andes (Pfeffer et al., 2014) and have been shown to be sensitive indicators of

¹Instituto de Geografía, Pontificia Universidad Católica de Chile, Chile

²Department of Geology, University of Cincinnati, USA

³Department of Earth Science, Dartmouth College, USA

⁴Department of Geography, The University of Utah, USA

⁵Convenio Gaia Antártica, Universidad de Magallanes, Chile

⁶Department of the Geophysical Sciences, University of Chicago, USA

Corresponding author:

Esteban A Sagredo, Instituto de Geografía, Pontificia Universidad Católica de Chile, Santiago 782-0436, Chile.

Email: esagredo@uc.cl

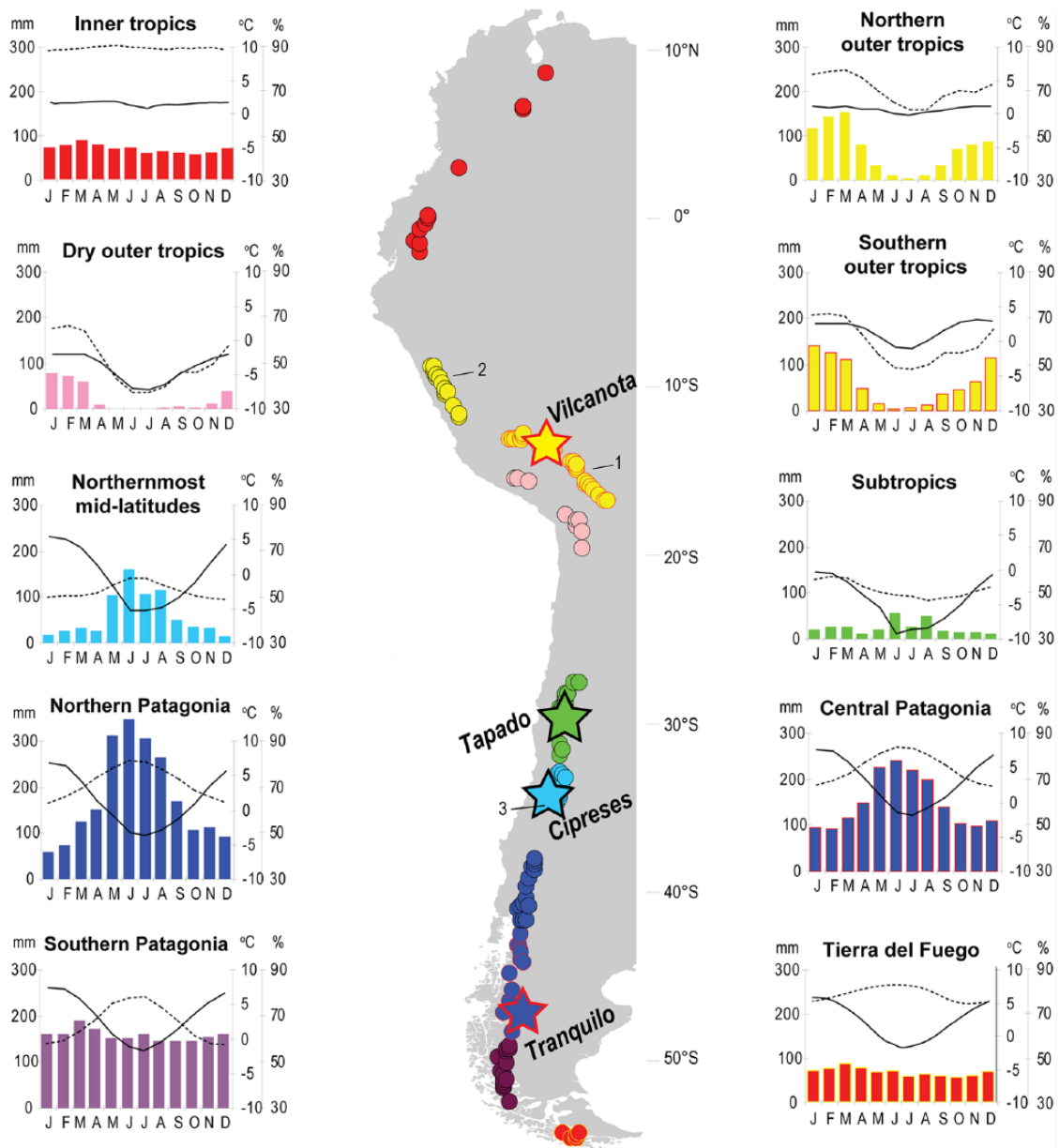


Figure 1. Classification of Andean glaciers (modified from Sagredo and Lowell, 2012). The sample includes 234 glaciers distributed throughout the Andes ($12^{\circ}30'N$ – $55^{\circ}S$). Each dot represents a single glacier. Plots (in matching colors) represent mean climatic conditions within each group. The horizontal axis represents the month of the years. The bars represent monthly precipitation (mm), solid lines show mean monthly temperature ($^{\circ}C$), and dashed lines represent mean monthly humidity (%). All climatic information was extracted from CRU CL 2.0 climate model, $10'$ latitude/longitude resolution (New et al., 2002). Study sites are represented by the stars. Numbers represent sites used in the discussion (1: Cordillera Real, Bolivia; 2: Cordillera Blanca, Peru; and 3: El Peñón and El Azufre glaciers, Argentina).

climate change (Dyurgerov and Meier, 2000; Leclercq et al., 2014). Unfortunately, the records of glacial fluctuations during the last millennium in the Southern Hemisphere are relatively scarce and have an uneven spatial distribution (Grove, 2004; Jomelli et al., 2009; Masiokas et al., 2009). Furthermore, reconstructing past climates based on the glacial record has been hindered because it has been shown that glaciers located in different climatic regimes may respond with differing magnitudes to similar climatic perturbations (Favier et al., 2004; Kaser, 2001; Sagredo et al., 2014; Seltzer, 1994).

Here, we outline an approach to address these issues and reconstruct climate scenarios during the last millennium (temperature and precipitation), using alpine glaciers located in four different climatic regimes along the Andes. With this study, we aim to understand the spatial variability of equilibrium line altitude (ELA) changes and associated climate conditions during this time period. A comprehensive mapping of these variables, based

on network of sites and along a wide range of latitudes, is critical for testing hypotheses regarding the mechanisms underlying the glacial events that occurred during the last millennium.

Study areas

The Andes extend for 9000 km through western South America, spanning a broad range of latitudes and altitudes, which in turn encompasses a large range of climatic conditions (Garreaud et al., 2009). Based on statistical analyses (i.e. cluster and principal component analysis) of temperature, precipitation, and humidity, Sagredo and Lowell (2012) classified the glacierized regions of the Andes into seven distinct climatic groups (Figure 1). Modeling experiments show that each of these groups has a distinctive response to perturbations in temperature and precipitation (Sagredo et al., 2014). Here, we report on glacier reconstructions from four of these climatic groups: Cordillera Vilcanota ($13^{\circ}S$)

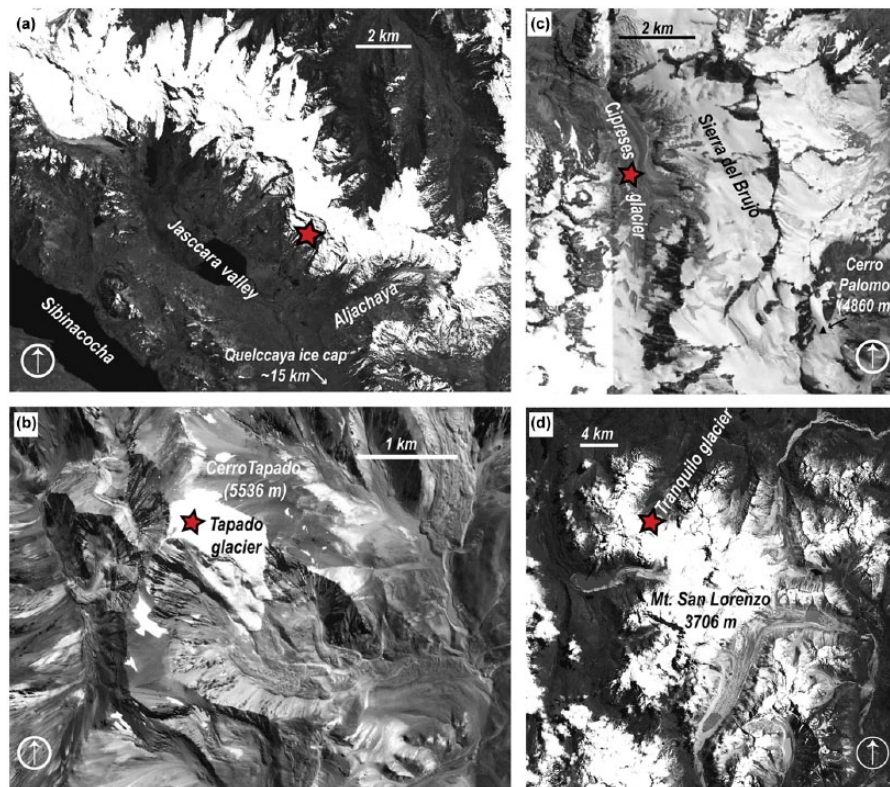


Figure 2. Study sites: (a) Cordillera Vilcanota, (b) Cerro Tapado, (c) Río Cipreses valley, and (d) Río Tranquilo valley. Stars show the specific location of the study areas.

Table 1. Summary of the main characteristics of the study sites. Climate groups following Sagredo and Lowell (2012). We also included the range of AAR values used to calculate the present and late-Holocene ELAs (see the ‘Methods’ section).

Site	Latitude	Longitude	Range of elevation (m)	Length (km)	Surface (km ²)	Aspect	Climatic group (Sagredo et al., 2012)	AAR range
Vilcanota	13°48’S	70°59’W	5070–5450	1.3	0.74	SW	Southern outer tropics	0.7–0.8
Tapado	30°08’S	69°55’W	4700–5536	1.5	1.2	SEE	Subtropics	0.4–0.5
Cipreses	34°34’S	70°21’W	2580–4340	10.5	21	N	N. mid-latitudes	0.55–0.65
Tranquilo	47°33’S	72°23’W	1270–2200	2.2	2.7	NE	Central Patagonia	0.55–0.65

AAR: accumulation area ratio; ELA: equilibrium line altitude.

located in the outer tropics, Tapado glacier (30°S) in the subtropics, Cipreses glacier (34°S) in northernmost mid-latitudes, and Tranquilo glacier (47°S) in central Patagonia (Figures 1 and 2). These glaciers were part of the sample used by Sagredo and Lowell (2012) to define the climate groups, and are considered to be climatically representative of their region. To minimize local influences, these sites were selected based on the following criteria: (1) small valley glaciers, with faster response time to climate change; (2) simple geometry, minimizing the number of tributaries; (3) accessibility; and (4) independence from major ice bodies (i.e. ice fields or ice caps). Table 1 summarizes the main characteristics of the study sites.

Cordillera Vilcanota

The Cordillera Vilcanota (13°45’S, 71°05’W) is a small mountain range that extends east-west for almost 50 km and forms part of the eastern Cordillera of the southern Peruvian Andes (Mark et al., 2002) (Figure 1). Its highest peak is Nevado Ausangate (6372 m a.s.l.). The climate in this area is characterized by a single marked wet season during the austral summer months (DJFM) and a prolonged ablation season (Rodbell et al., 2009).

Approximately 15 km to the southwest, at Quelccaya Ice Cap (the largest ice mass in the tropics), systematic meteorological observations at 5680 m a.s.l. have shown that the mean annual temperature in this area is approximately -4.1°C (2004–2013) (D. Hardy, 2015, personal communication) and that mean annual accumulation is 0.86 ± 0.15 m water equivalent (2005–2015) (Hurley et al., 2015). The Cordillera Vilcanota is composed of granitic, sedimentary, and volcanic rocks (Audebaud, 1973). Our study focused on a small valley glacier in the Jaccara Valley (13°48’S, 70°59’W; herein Vilcanota site, Figure 2a), located in the southeastern Cordillera Vilcanota. With an estimated area of 0.74 km², this alpine glacier is 1.3 km long and has a steep profile with elevations ranging from ~5450 to 5070 m a.s.l.. The ELA in the north side of the range is estimated at 5100 m a.s.l. (Mercer and Palacios, 1977), just 30 m above the toe of the modern glacier.

Tapado glacier, Cerro Tapado

Cerro Tapado (30°08’S, 69°55’W), with a maximum elevation of 5536 m a.s.l., is located south of the climatic region known as the Arid Diagonal (De Martonne, 1934) (Figure 1). Although high elevations at Cerro Tapado sporadically receive summer

precipitation from the southeast, most precipitation in this area is linked to winter cut-offs of cold air-masses from the Pacific (Ginot et al., 2002; Marengo et al., 2004; Vuille and Ammann, 1997). Despite being located in an arid and generally ice-free environment, the southeast slope of Cerro Tapado hosts an ~1.5-km-long glacier (Schotterer et al., 2003) (Figure 2b), which reaches elevations as low as 4700 m a.s.l. With a surface area of ~1.2 km², this glacier is the largest ice mass in the area. It has an estimated ELA of 5300 m a.s.l. (Kull et al., 2002). The forefield of Tapado glacier is occupied by several rock glaciers of different ages.

Cipreses glacier, Sierra del Brujo

Sierra del Brujo (34°36'S, 70°17'W) is a small range located in central Chile, in the transition zone between the arid Andes and extremely wet Patagonia (Figure 1). The region exhibits mild, wet winters (~4 months long) and dry summers. Summers are semi-permanently affected by a high-pressure cell over the southeast Pacific Ocean, which prevents precipitation belts from reaching the area. During the winter, the westerlies can reach this region and generate frontal and orographic precipitation (Bown et al., 2008). The closest meteorological station located in Sewell (34°05'S, 70°24'W, 2155 m), 40 km north of Sierra del Brujo, reports a mean annual temperature of 10.4°C and total annual precipitation of 891 mm (Dirección Meteorológica de Chile, 2001). The Sierra del Brujo, composed of granodioritic rocks, is one of the most glacierized regions in the Central Andes of Argentina and Chile. This study focuses on Cipreses glacier (34°34'S, 70°21'W; Figure 2c), which extends north-south for ~9 km through the middle of Sierra del Brujo, with elevations ranging from ~4340 to 2580 m a.s.l. Including tributary glaciers, Cipreses glacier comprises an area of ~21 km². The lower portion of the glacier is debris-covered. No information regarding the ELA has been estimated for this or other glaciers in the area.

Tranquilo glacier, Monte San Lorenzo

Monte San Lorenzo (47°35'S, 72°19'W) is an isolated granitic massif located ~70 km to the east of the southern limit of the Northern Patagonian Icefield, more than 165 km from the coast (Figure 1). This mountain is the third highest summit in the southern Andes with an elevation of 3706 m a.s.l. The Monte San Lorenzo area has a transitional maritime to continental climate with a wide-annual thermal amplitude and a narrow range of mean monthly precipitation (Falaschi et al., 2013). The closest meteorological station located in Cochran (47°14'S, 72°33'W, 182 m a.s.l.), 30 km to the northwest of Monte San Lorenzo, reports a mean annual temperature of 8.1°C and total annual precipitation of 731 mm (Aravena, 2007).

Monte San Lorenzo is one of the most extensively glacierized mountains in the region, with an ice-covered area of ca. 139 km² (Falaschi et al., 2013). Based on satellite images from 2005 to 2008, Falaschi et al. (2013) estimated the snowline to be ~1700–1750 m a.s.l. on the western sector of the massif and ~1800 m a.s.l. on the eastern side. This study focuses on Río Tranquilo valley, a north-south oriented valley on the northern flank of Monte San Lorenzo. A recent glacier inventory shows the existence of 16 small glaciers (<5 km²) in the headwalls of the valley, adding a total ice surface of 15 km² (Falaschi et al., 2013).

Methods

Glacier reconstruction and chronology

Former glacier extents and paleo-glacier surfaces were reconstructed using moraines and trimlines. We analyzed aerial photographs, satellite imagery (ASTER, Quickbird), and digital

elevation models (ASTER GDEM Worldwide Elevation Data) to identify and map glacial landforms (for details, see Supplementary material, Appendix 1, available online). All remote interpretations were field checked.

To constrain the age of the former glacial fluctuations, we determined direct ages of moraines using surface exposure (¹⁰Be and ³⁶Cl) dating. At the Vilcanota site, and Cipreses and Río Tranquilo glaciers, we collected rock samples (~1 kg) for ¹⁰Be measurements from the surface of boulders atop moraine crests. Our sampling focused on large boulder (preferably >1 m), well embedded in the moraine, and that did not show evidence of post-depositional movement, surface erosion, or exhumation (see Supplementary material, Appendix 2, available online). Samples were removed from boulder surfaces (upper 5 cm) using a hammer and chisel or the drill and blast method of Kelly (2003). Beryllium was isolated from whole-rock samples in the cosmogenic laboratory at Dartmouth College. ¹⁰Be/Be isotope ratios were measured at the Center for Accelerator Mass Spectrometry at Lawrence Livermore National Laboratory (CAMS LLNL). ¹⁰Be ages were calculated based on the methods incorporated in the CRONUS-Earth online exposure age calculator version 2.2, with version 2.2.1 of the constants file (Balco et al., 2008). ¹⁰Be ages were calculated using the Southern Hemisphere mid-latitude ¹⁰Be production rate documented by Putnam et al. (2010) in New Zealand, which has been shown to be valid for sites in Patagonia (Kaplan et al., 2011), as well as for high-altitude tropical locations (Kelly et al., 2015). ¹⁰Be ages were calculated with time-dependent scaling after Lal (1991) and Stone (2000), although other scaling schemes (Desilets and Zreda, 2003; Dunai, 2001; Lifton et al., 2008; Pigati and Lifton, 2004) agree within 5% (not shown). All ¹⁰Be ages were calculated assuming no erosion. This assumption is likely valid giving the relatively young moraine ages and since selected boulders exhibiting minimal evidence of erosion. ¹⁰Be exposure ages are shown and discussed with analytical errors only.

In the case of Tapado glacier, where the predominant rock type is quartz poor, we determined moraine ages using ³⁶Cl dating. The moraines were barren of large boulders, and therefore, we opted to sample cobbles (~10 cm in diameter) from the surfaces of moraine ridges and other geomorphic features. This approach has been shown to yield cosmogenic ages indistinguishable from those collected from boulders on the same moraine, if collected where exhumation from depth or temporary burial of the cobbles is unlikely (Briner, 2009). To determine the whole-rock chemistry of the samples, we conducted elemental analysis at Activation Laboratories, Ltd. (ON, Canada; see Supplementary material, Appendix 3, available online). Cl samples were processed and ³⁶Cl ratios and total chloride were measured by isotope dilution and accelerator mass spectrometry (AMS) at Purdue Rare Isotope Measurement (PRIME) Laboratory at Purdue University. Ages were calculated using the CRONUSCalc ³⁶Cl online exposure age calculator, Version 2.0 (Marrero et al., 2016) using the Lifton-Sato-Dunai (LSD) nuclide-dependent scaling scheme (Lifton et al., 2014), which has been shown to produce ³⁶Cl ages that agree well with similarly scaled, locally calibrated Holocene ¹⁰Be and radiocarbon ages at high-altitude, low-latitude sites (Phillips et al., 2016). To check the consistency between ³⁶Cl and ¹⁰Be ages reported, we also calculated the ³⁶Cl ages using a time-varying Lal (1991)/Stone (2000) scaling scheme, which yielded identical ³⁶Cl ages to the LSD scheme (within 1.2% on average, and well within analytical uncertainty). Only sample ages calculated with the LSD scaling scheme are reported here. We note that calibration sites for ³⁶Cl production rates, particularly for whole-rock samples in this age range, are sparse (Phillips et al., 2016), so all input variables are provided in CRONUSCalc format in the data repository for ease of recalculation using other schema and calibration datasets as they become available. All ³⁶Cl ages were

calculated assuming zero erosion. We interpret all surface exposure (^{10}Be and ^{36}Cl) ages presented as the start of glacial retreat from the moraine from which the sample was collected.

Additionally, at the Vilcanota site, we collected radiocarbon samples from organic remains embedded in a moraine ridge. Radiocarbon measurements were carried out at the National Ocean Science Accelerator Mass Spectrometry Facility (NOSAMS). All radiocarbon ages were converted to calendar years BP (cal yr BP) using CALIB 7.02 and the SHCal13 calibration curve (Reimer et al., 2013). After calibration, radiocarbon ages discussed in this paper were corrected in order to make them comparable to our cosmogenic dates; this implies using the year 2010 as our reference for the present (CE 1950 + 60 yr = CE 2010).

For this analysis, to make consistent comparisons, we focused on the most extensive glacial advance (outermost moraines) that occurred during the last millennium, as identified by our chronology. Hereinafter, we refer to this event as the last millennium maximum (LMM), recognizing that the timing of this event may differ among the study areas.

Modern and paleo-ELAs

Paleo-glacier surfaces were reconstructed based on marginal features that indicate the past extents of the glacier and the elevations of its former margins. We paid particular attention to identify geomorphic evidence indicating the presence of tributary glaciers that may have merged with the main glacier during the LMM. Such evidence would have an important impact on the reconstruction of paleo-surfaces and, in turn, on the calculation of the basin's hypsometry. Finally, we reconstructed the LMM glacier surface by fitting a planar surface over the former margins of the glacier. This approximation, although it does not capture the typical glacier surface topography (i.e. convex near the terminus, horizontal at mid-elevations, and concave near the headwall), can be considered a first-order approximation. The hypsometry of the glaciers was calculated based on the ASTER GDEM2 Worldwide Elevation Data (1.5 arc-second resolution). Present-day ice extents were mapped using Google Earth images taken in 2013 and 2015 (see Supplementary material, Appendix 1, available online).

To determine modern and former ELAs, we apply the accumulation area ratio (AAR) method, which assumes that the accumulation area of a glacier occupies a fixed portion of a glacier's total area (Porter, 2001). The ELA is calculated by applying an estimated AAR value to a hypsometric curve of the glacier. Thus, this method is not only easy to apply but also takes into consideration the hypsometry of the glaciers in the ELA estimation.

The AAR values, however, vary from one region to another (Benn et al., 2005; Benn and Lehmkühl, 2000). For example, steady-state AAR values for mid- and high-latitude glaciers range from 0.5 to 0.8 (Meier and Post, 1962), with typical values between 0.55 and 0.65 (Porter, 1975). AAR values tend to be higher for the inner tropics (AAR = ~0.8, Kaser and Osmaston, 2002). To accommodate this issue, we calculated the ELA values using a range of ratios derived from previous studies (Table 1). For our tropical site, Cordillera Vilcanota, we used AAR values ranging from 0.7 to 0.8, which are considered representative for tropical glaciers (Kaser and Osmaston, 2002). For Tapado glacier, in the subtropics, based on recent mass balance data (Kinnard, C., 2012, personal communication) and modeling results (Kull et al., 2002), we used AAR values ranging from 0.4 to 0.5. Finally, for the two mid-latitude glaciers, Tranquilo and Rio Cipreses, we applied the range of AAR values most commonly used for mid-latitude glaciers of 0.55–0.65 (Bahr et al., 2009; Porter, 1975).

The AAR method was designed to calculate ELAs for glaciers under steady-state conditions. Thus, the calculations of ELAs of modern glaciers, which we consider to reflect 'transient'

conditions, are likely lower than the actual ELA. Calculating the offset between the transient (minimum) ELA value and the actual ELA value is outside the scope of this study, but might be the subject of future work.

The change in ELA was calculated by subtracting the modern ELA from the paleo-ELA, using the mean, minimum, and maximum AAR values estimated for each zone. This method assumes that the AAR value for each glacier remains the same from the LMM to the present. We also assumed that the differences in glacial extent and ELA among sites are driven by mean climatic conditions and not simply by stochastic climate variability.

We recognize that debris-covered glaciers exhibit a complex interaction with climate (e.g. Reid and Brock, 2010). ELA calculations could be affected by this issue; debris cover reduces ablation and can affect glacial response on short time-scales. However, only one of our study sites (Cipreses glacier) currently exhibits debris cover. Since this debris cover occupies less than 10% of the total ice surface, we suggest that its impact on our conclusions is negligible.

Paleoclimatic reconstruction

The difference between the modern and LMM ELAs provides the basis to reconstruct scenarios of climatic conditions (temperature and precipitation) using a surface energy and mass balance model (SEMB model; Rupper and Roe, 2008). Details, uncertainties, and validation of the SEMB model can be found in Rupper and Roe (2008) and Sagredo et al. (2014). Below we briefly summarize the model.

For a given set of climatic conditions at a location, the SEMB model uses nested surface energy balance and surface mass balance algorithms to seek the altitude at which there is both a surface energy balance and a mass balance, defined here as the modeled ELA. The surface energy balance model solves for the energy available for ablation at a monthly resolution, using the following equation:

$$Q_m = S + L + Q_s + Q_l$$

where Q_m is the energy available for melting snow/ice, S is the shortwave radiation flux absorbed at the surface, L is the net longwave radiation flux, Q_s is the sensible heat flux, and Q_l is the latent heat flux. Heat conduction is neglected because it is likely small compared with the terms we considered (Kayastha et al., 1999). The detailed equations describing S , L , Q_s , and Q_l can be found in Rupper and Roe (2008) and correspond to energy balance equations commonly employed in glaciology (e.g. Cuffey and Paterson, 2010; Kayastha et al., 1999; Mölg and Hardy, 2004; Plummer and Phillips, 2003; Senese et al., 2012).

The surface energy balance algorithm seeks a surface temperature that balances the given monthly air temperature, such that surface shortwave radiation is equal to outgoing longwave radiation and turbulent heat fluxes. If the resulting surface temperature is less than zero, then melt is zero and sublimation is proportional to the turbulent latent heat flux. If the surface temperature is zero, then both melt and sublimation are zero. Finally, if the surface temperature required to achieve energy balance is greater than zero, then the surface temperature is forced back to zero and the excess energy is used to calculate total melt.

The total annual ablation is calculated as the sum of the monthly sublimation and melt. In the surface mass balance algorithm, the model seeks the air temperature whereby total annual ablation equals annual accumulation. The ELA is found by using the local lapse rate to calculate the altitude at which this air temperature lies. The local temperature lapse rate was calculated based on the difference between the temperature at the geopotential height closest to the surface and the temperature at the geopotential height one

Table 2. List of the model variables and units used.

Variables		Units
<i>CRU CL 2.0</i>		
Ta_2m	Monthly mean annual 2 m air temperature	°C
Acc	Monthly mean precipitation	m
RH	Relative humidity	%
v	Wind speed	m s ⁻¹
<i>NCEP-NCAR</i>		
Ta_std	Standard deviation of monthly 2 m air temperature	°C
Acc_std	Standard deviation of monthly mean precipitation	m
P	Air pressure at surface	Pa
Swdown	Net incoming shortwave radiation at the surface	W m ⁻²
LWdown	Downwelling longwave radiation	W m ⁻²
Ta_GP	Pressure level temperature	°C
H_GP	Pressure level Geopotential Height	m
Elev	Elevation of the grid cells	m

NCEP-NCAR: National Centers for Environmental Prediction–National Center for Atmospheric Research.

level higher, using National Centers for Environmental Prediction–National Center for Atmospheric Research (NCEP-NCAR) reanalysis data as input (Kalnay et al., 1996).

Here, we solve for the suite of combined temperature and precipitation perturbations that accommodate the ELA change since the LMM. Model parameters and constants are the same as in Sagredo et al. (2014).

For all required SEMB model climate inputs, we used gridded monthly climatologies from the period 1961–1990. In particular, we used the gridded climatological output from CRU CL 2.0 (New et al., 2002) (Table 2). CRU CL 2.0 is a 10' latitude/longitude resolution dataset of mean monthly surface climate over global land areas, interpolated from station means for 1961–1990. This dataset provides high-resolution information regarding those climatological variables (2-m air temperatures, annual precipitation, relative humidity, and wind speed) that are likely sensitive to local conditions. Unfortunately, this dataset does not provide all necessary inputs for the SEMB model. The remaining inputs were obtained from the NCEP-NCAR reanalysis output (Kalnay et al., 1996) (Table 2). NCEP-NCAR reanalysis uses an analysis/forecast system to perform data assimilation (2.5° resolution) using past data from 1948 to the present. The monthly mean reanalysis output for the period 1961–1990 was linearly interpolated to a 10' resolution, thus providing the monthly climatologies consistent with the CRU input data used. Although uncertainty exists with these datasets, especially at high elevations, Sagredo et al. (2014) showed that the combined use of high-resolution CRU CL 2.0 climatological data and NCEP-NCAR reanalysis output, applied to our SEMB, captures the spatial pattern of modern ELAs across the Andes.

Results

LMM reconstruction

Below, we describe the general glacial geomorphology and chronology used to define past glacial extents at the four study areas, with a focus on the features interpreted to date to the LMM.

Vilcanota site. Geomorphic evidence suggests that glaciers ice in the Jascara basin expanded and deposited a series of moraines on the valley walls and bottom. We identified at least six moraine complexes in the area (Figure 3a). The Jascara I and II moraines are associated with advances of the glaciers at the headwalls of the basin (9 and 7 km upvalley). The Tributary I, II, and III moraine complexes are the result of glacial fluctuations of the

small tributary valleys on the northeast slope of the Jascara valley. The Aljachaya moraine complex, on the other hand, was deposited by a glacier flowing out of the Aljachaya valley.

We obtained two radiocarbon dates of peat embedded in the outermost ridge of the Tributary I moraine. One age from the top and one from the bottom of this peat deposit yield ages of 560–590 and 1120–1330 cal yr BP, respectively (Table 3). These ages suggest that peat was growing upvalley from the Tributary I moraines during these times and that ice was smaller than the Tributary I extent from ~1330 to 560 cal yr BP. The peat was likely incorporated into the moraine after ~560 cal yr BP as the glacier advanced over the area where the peat was growing. Thus, these dates represent maximum-limiting ages for the Tributary I moraines. These dates agree with four samples from boulders on the crest of the Tributary I moraines that yield ¹⁰Be ages of 720 ± 20, 310 ± 10, 240 ± 20, and 160 ± 10 yr BP (Tables 4 and 5, and Figure 4a), with progressively younger ages more proximal to the glacier. These ages constrain the timing of glacier retreat from the Tributary I moraine. Based on these data, we suggest that the Tributary I moraines mark the LMM ice extent at the Vilcanota site and that this occurred at <560 yr BP. Similar dates constrain the LMM at Quelccaya Ice Cap, confirming our findings (see section 'Discussion'; Stroup et al., 2014, 2015).

Tapado glacier. As is common in lower precipitation regions, landforms below the glacier accumulation area also include mass wasting features. Debris-covered ice, ice-cored moraines, lobulated (and lineated) terrain, and several generations of massive rock glaciers occupy the forefield of Tapado glacier (Figure 3b). We distinguished a series of semi-continuous conspicuous moraine ridges (1–4 m high) that form an elongated arch in the forefield of Tapado glacier (Figure 3b, in pink) that appear to have undergone minimum disturbances since formation. We interpret this unit (herein: Tapado I) as a moraine complex formed by an advance of Tapado glacier over debris-covered ice. Distal to the Tapado I moraines are remnants of at least three or four older lateral moraines (Figure 3b, in fuchsia).

Four ³⁶Cl samples collected from the crest of Tapado I moraines yield ages of 490 ± 130, 540 ± 70, 950 ± 90, and 1830 ± 270 yr BP (Table 6, Figure 4b). One ³⁶Cl sample collected from the surface of an ice-cored moraine, just outside of the Tapado I moraine, resulted in an age of 780 ± 100 yr BP. Samples from the lateral Tapado II moraines yielded ages of 3040 ± 330 and 5100 ± 290 yr BP. Despite the scatter in these dates, we can distinguish at least two groups of ages: one group associated with the Tapado I moraine, with ages ranging between 500 and 1000 yr BP (one outlier), and another group associated with the Tapado II moraines, with two ages that are considerably older. Based on these results, we suggest that the Tapado I moraine was deposited sometime during the first half of the last millennium and that it represents the LMM limit. The Tapado II moraine, on the other hand, was probably deposited by a single or multiple glacial advances during the Holocene, prior to the deposition of Tapado I (the scatter of the ages precludes further interpretation)

Cipreses glacier. The upper section of the valley exhibits abundant evidence of former fluctuations of Cipreses glacier. We identified at least four past ice extents, marked by the Medina II, Medina I, Arriero, and Alto Cipreses moraine complexes (Figure 3c). These moraines are located approximately 5, 4.5, 2.7, and 2 km from the present-day ice margin, respectively.

The outermost complex, Medina II, includes two sets of moraines that occur only on the valley walls. Approximately 1.5 km upvalley, Medina I complex is also formed by two sets of moraines, ~50 m apart. The outermost Medina I is a single ridge, ~1.5 m high. The inner Medina I moraines comprise at least 5 cross-cutting ridges 3–5 m high. The Medina I moraines are

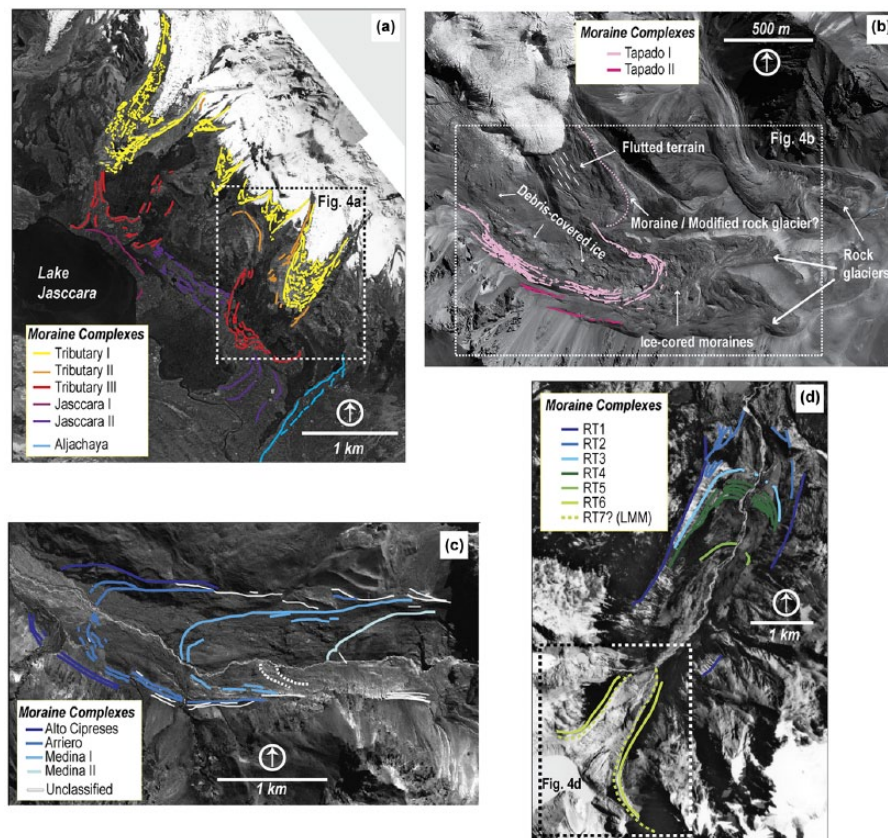


Figure 3. Moraine complexes: (a) Cordillera Vilcanota, (b) Cerro Tapado, (c) Río Cipreses valley, and (d) Río Tranquilo valley. Each line represents an individual moraine ridge. Considering the complexity of the landscape in the forefield of Tapado glacier, other geomorphic units were also identified in panel (b). The dashed line in panel (d) represents a subtle ridge plastered against the inner slope of the RT6 moraine complex; we suggest that this subtle ridge corresponds to the LMM.

Table 3. AMS radiocarbon and calibrated ages from Vilcanota. All radiocarbon dates were converted to calendar years BP using CALIB 7.02 and the SHCal13 calibration curve (Stuiver and Reimer, 1993).

Sample	Lat. (°S)	Long. (°W)	Lab code	Material	$\delta^{13}\text{C}$ value (‰)	^{14}C yr BP $\pm 1\sigma$	Median prob. (cal yr BP)	2σ range (cal yr BP)
PEc10-01-01	-13.816	-70.968	OS-84284	Peat	-26.35	1260 \pm 35	1130	1060–1270
PEc10-01-04	-13.816	-70.968	OS-84200	Peat	-23.04	500 \pm 20	510	500–530

AMS: accelerator mass spectrometry.

dissected and partially buried by outwash. The next younger moraine complex, the Arriero moraines, consists of two very well-defined moraines and a series of discontinuous and subdued inner ridges. The Alto Cipreses moraine is a single ridge, ~3 m high, located in the northern side of the river (Figure 3). It is characterized by a lack of matrix and an abundance of large boulders (>1.5 m high). The boulders atop all the moraine complexes lack lichens and do not exhibit evidence of post-depositional erosion.

We obtained ^{10}Be samples from boulders located atop all four moraine complexes (Tables 4 and 5, and Figure 4c). Next, we describe our chronological results from the stratigraphically oldest moraine complex to the youngest. Two ^{10}Be samples from the Medina II moraine complex yield ages of 950 ± 40 and 760 ± 50 yr BP. Immediately proximal to this, three ^{10}Be samples from Medina I moraines yield ages of 950 ± 50 , 780 ± 50 , 640 ± 40 , and 580 ± 30 yr BP. Given the cluster of ages that range from 580 ± 30 and 950 ± 50 yr BP, we suggest that Medina I and Medina II moraines were deposited during the first half of the last millennium. The present data, however, do not allow us to distinguish these two moraine groups. Upstream, two ^{10}Be samples from the innermost Arriero moraine yield ages of 8050 ± 150 and 630 ± 30 yr BP. While the youngest of these ages falls within the spread of the ages of

the Medina I and Medina II moraines, the other is apparently too old, based on the young stratigraphic position of this moraine, and we consider it an outlier. Finally, two samples from Alto Cipreses moraine complex yield ages of 2160 ± 70 and 1270 ± 50 yr BP. The abundance of large clasts and the lack of a fine matrix in this moraine may suggest that this landform was formed from a rockfall on the glacier surface, which was later transported to the ice margin, therefore providing ages older than the time of moraine deposition. Finally, one ^{10}Be sample, collected from a ridge of unconsolidated sediments (of unknown origin) ~100 m distal to the Medina II moraine complex, yielded an age of $15,020 \pm 280$ yr BP. This age could either correspond to an outlier or confirm that the Medina II moraines represent the LMM. We favor the latter interpretation, as the distal ridges exhibit significant differences in weathering and vegetation. We suggest that collectively these data indicate that the Cipreses glacier was expanded during the first half of the last millennium (between ~950 and 550 yr BP) and that Medina II moraines represent the most extensive advance of the Cipreses glacier since 15,020 yr BP (Tables 4 and 5, and Figure 4c). Note that this chronology differs from previous interpretations (Le Quesne et al., 2009; Röthlisberger, 1987), a matter addressed in the discussion.

Table 4. Geographical and analytical data for ^{10}Be samples. Ratios are normalized to the 07KNSTD standard. Shown are 1σ analytical AMS uncertainties. Density = 2.6 gm/cm^3 . Samples were prepared at Dartmouth College. Carrier concentration = 1.314 ppt .

Sample ID	CAMS number	Latitude ($^{\circ}\text{S}$)	Longitude ($^{\circ}\text{W}$)	Elevation (m asl)	Boulder height (cm)	Thickness (cm)	Shielding	Quartz wt. (g)	^9Be Carrier (g)	$^{10}\text{Be}/^9\text{Be} \pm 1\sigma$ (10^{-14})	^{10}Be Conc. $\pm 1\sigma$ (10^3 at g^{-1})
<i>Vilcanota</i>											
PE10-01-02	BE32436	-13.8129	-70.9679	5016	180	2.1	0.994367	13.1379	0.1587	0.6222 ± 0.0461	6.60 ± 0.49
PE10-01-03	BE32437	-13.8136	-70.9679	5015	160	1.9	0.994983	12.9529	0.1625	0.8889 ± 0.0620	9.79 ± 0.68
PE10-01-05	BE32438	-13.8160	-70.9683	4959	80	1.8	0.988513	16.6620	0.1635	1.4529 ± 0.0644	12.52 ± 0.55
PE10-01-06	BE32439	-13.8157	-70.9690	4968	80	1.4	0.987221	12.9576	0.1627	2.6716 ± 0.0996	29.45 ± 1.10
<i>Gprieses</i>											
CC10-01-02	BE32414	-34.5470	-70.4202	1730	182	4.8	0.962666	17.1747	0.1627	1.0149 ± 0.0660	8.45 ± 0.55
CC10-01-03	BE32407	-34.5463	-70.4206	1705	70	2.5	0.964482	20.2736	0.1626	1.4782 ± 0.0805	10.42 ± 0.57
CC10-01-05	BE32415	-34.5459	-70.4194	1707	95	1.5	0.970388	20.2923	0.1626	0.9927 ± 0.0709	6.99 ± 0.50
CC10-01-06	BE32416	-34.5505	-70.3948	2018	140	2.6	0.939738	31.2031	0.1622	6.2949 ± 0.2123	28.75 ± 0.97
CC10-01-09	BE32417	-34.5508	-70.3951	1983	100	3.5	0.945451	23.6607	0.1648	2.7142 ± 0.1065	16.61 ± 0.65
CC10-01-10	BE32408	-34.5489	-70.4094	1798	100	2.0	0.965425	22.7830	0.1619	16.4457 ± 0.3120	102.69 ± 1.95
CC10-01-11	BE32409	-34.5489	-70.4092	1793	110	2.5	0.965281	33.7317	0.1621	1.6962 ± 0.0852	7.16 ± 0.36
CC10-01-12	BE32410	-34.5448	-70.4255	1712	150	3.0	0.948674	23.6899	0.1618	1.7102 ± 0.0861	10.26 ± 0.52
CC10-01-13	BE32411	-34.5468	-70.4247	1760	70	4.1	0.960604	23.5803	0.1621	1.3988 ± 0.0979	8.45 ± 0.59
CC10-01-14	BE32418	-34.5478	-70.4194	1722	230	2.5	0.962559	27.5314	0.1622	1.2056 ± 0.0786	6.24 ± 0.41
CC10-01-19	BE32412	-34.5390	-70.4200	1772	110	2.5	0.974641	34.1962	0.1622	45.1592 ± 0.8426	188.22 ± 3.51
<i>Tranquilo</i>											
PC10-01-17	BE32431	-47.5278	-72.3912	1291	160	2.0	0.984082	27.5379	0.1623	12.6183 ± 0.2429	65.30 ± 1.26
PC10-01-18	BE32432	-47.5273	-72.3912	1281	100	1.3	0.977047	35.7078	0.1620	16.7384 ± 0.4178	66.68 ± 1.66
PC10-01-19	BE32433	-47.5270	-72.3912	1277	110	2.7	0.980356	37.7215	0.1616	16.4104 ± 0.3069	61.73 ± 1.15

AMS: accelerator mass spectrometry.

Table 5. ^{10}Be ages (yr BP) from Vilcanota, Cipreses, and Tranquilo sites. Ages calculated based on methods incorporated in the CRONUS-Earth online exposure age calculator, version 2.2, with version 2.21 of the constants file (see text, Balco et al., 2008), which includes renormalization of Table 3 results relative to 07KNSTD (Nishiizumi et al., 2007). Ages were calculated using the time-dependent version of Stone/Lal scaling scheme (Lal, 1991; Stone, 2000) with the production rate of Putnam et al. (2010). We report internal and external uncertainties that include scaling to the latitude and altitude of the sites.

	Sample	Age	int	ext
Vilcanota	PE10-01-02	160	10	10
	PE10-01-03	240	20	20
	PE10-01-05	310	10	20
	PE10-01-06	720	20	30
Cipreses	CC10-01-02	780	50	50
	CC10-01-03	950	50	60
	CC10-01-05	640	40	50
	CC10-01-06	2160	70	90
	CC10-01-09	1270	50	60
	CC10-01-10	8050	150	230
	CC10-01-11	630	30	30
	CC10-01-12	950	40	50
	CC10-01-13	760	50	60
	CC10-01-14	580	30	40
	CC10-01-19	15020	280	430
Tranquilo	PC10-01-17	5520	100	160
	PC10-01-18	5690	140	190
	PC10-01-19	5330	100	150

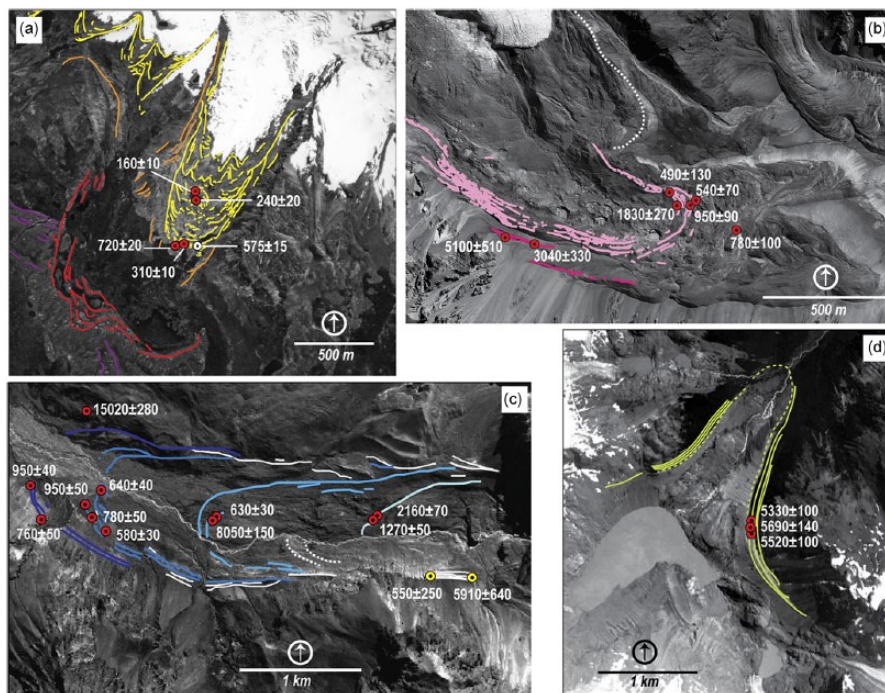


Figure 4. Dates constraining the age of the most prominent glacial advance that occurred during the Last Millennium Maximum (LMM) at each study site: (a) Cordillera Vilcanota, (b) Cerro Tapado, (c) Río Cipreses valley, and (d) Río Tranquilo valley. Red and white circles represent the location of the cosmogenic (ka) and radiocarbon ages (range of cal yr BP) obtained in this study, respectively. Yellow circles show the location of radiocarbon ages (cal yr BP) from Röthlisberger (1987).

Tranquilo glacier. Geomorphic evidence indicates that several small glaciers at the headwalls of Río Tranquilo valley expanded and coalesced in the past, forming a single Tranquilo glacier. This glacier flowed downvalley and deposited a series of moraines on the walls and bottom of the Río Tranquilo valley. At least six moraine complexes are well expressed in the valley (Figure 3d). The inner moraine (RT6) comprise between five and seven ridges that cross cut each other and enclose the valley ~ 3.5 km from the present ice margin (continuous light green lines in Figure 4d). Just inside RT6, we identified some small

remnants of moraine ridges (RT7; dashed line in Figure 4d). The area within these moraines exhibits little to no vegetation and soil development.

We collected three rock samples from boulders on a single ridge of the RT6. These samples yielded ^{10}Be ages of 5690 ± 140 , 5520 ± 100 , and 5330 ± 100 yr BP (Tables 4 and 5, Figure 4d). The consistency of these dates likely reflects that this moraine was deposited in a single event, and that the sampled boulders do not exhibit ^{10}Be inheritance. Furthermore, they indicate that any later ice extent was located within RT6. Based

Table 6. Geographical and analytical data and ages for the ^{36}Cl samples. Ages calculated using CRONUSCalc online calculator (Marrero et al., 2016) using Lifton-Sato-Dunai scaling (Lifton et al., 2014). We report external uncertainties.

Sample name	Sample Id	Latitude (°S)	Longitude (°W)	Elevation (m a.s.l.)	Thickness (cm)	Shielding	Cl in rock (ppm)	$^{36}\text{Cl}/\text{Cl}$ (10^{-15})	^{36}Cl concentration (10^5 at/g rock)	Age (years)
NC11-01-11	201201394	-30.1568	-69.91927	4423	2	0.976965	30.03482	62 ± 8	0.32 ± 0.06	490 ± 130
NC11-01-12	201201395	-30.1571	-69.91894	4543	6	0.979958	18.91351	187 ± 11	0.60 ± 0.05	1830 ± 270
NC11-01-21	201201396	-30.1584	-69.92498	4618	3	0.922875	20.35587	462 ± 21	1.60 ± 0.11	5100 ± 510
NC11-01-22	201201397	-30.1587	-69.92432	4612	5	0.944775	21.92102	318 ± 14	1.22 ± 0.08	3040 ± 330
NC11-01-30	201201398	-30.1573	-69.91828	4538	7	0.978667	10.5315	91 ± 5	0.17 ± 0.01	950 ± 90
NC11-01-32	201201399	-30.1573	-69.91814	4537	4	0.980437	12.68254	63 ± 3	0.14 ± 0.01	540 ± 70
NC11-01-33	201201400	-30.158	-69.91665	4526	6	0.984819	11.67535	98 ± 6	0.21 ± 0.02	780 ± 100

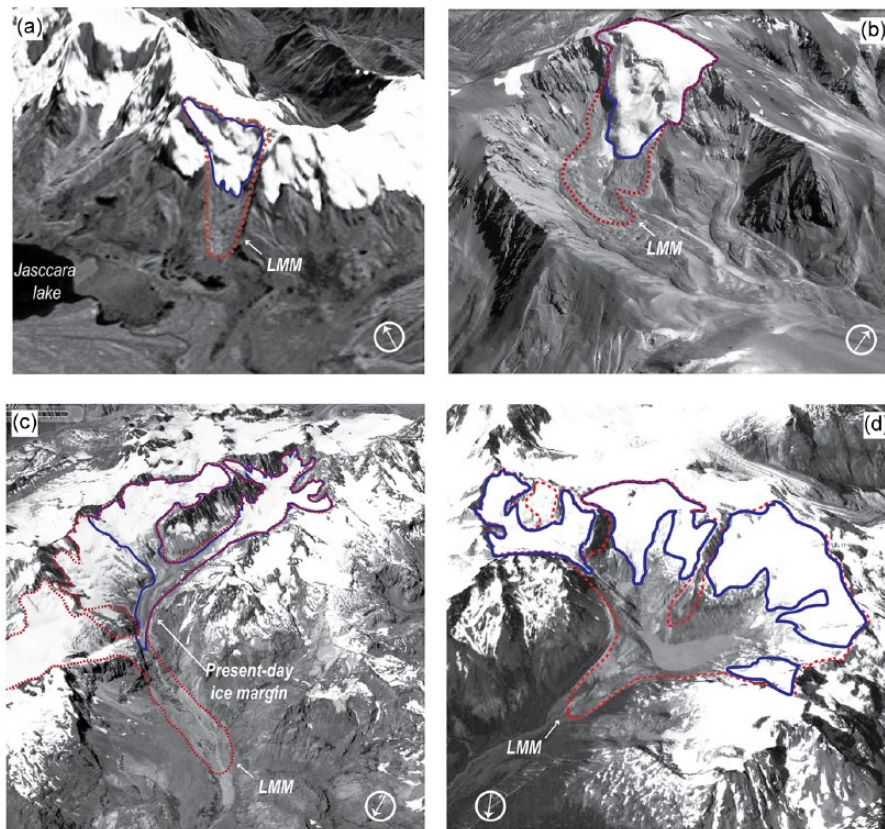


Figure 5. Oblique Google earth image showing the present-day (blue) and Last Millennium Maximum (red) ice margin: (a) Cordillera Vilcanota, (b) Cerro Tapado, (c) Rio Cipreses valley, and (d) Rio Tranquilo valley. Orientation of the images is shown by the circled arrows, which point to the North.

on this, we assume that the remnants of moraine ridges inside RT6 represent the LMM limit and use this glacier extent for subsequent ELA analysis. Because we did not find boulders suitable for ^{10}Be dating on these ridges, the age of the LMM is still unknown in the area.

Modern and paleo-ELAs

Based on the ice margins delineated in Figure 5, we estimated the present and LMM ELA for each glacier. Table 7 reports the ELAs corresponding to the preferred AAR value for each region. Figure 6 shows the range of ELA changes using the preferred AAR values.

We estimated the following ELA changes from the modern to the LMM: Vilcanota site 130–140 m, Tapado glacier 140–220 m, Cipreses glacier 100–160 m, and Tranquilo glacier 130–170 m. When comparing the magnitude of these ELA changes, only the estimates for Vilcanota and Tapado glacier do not overlap.

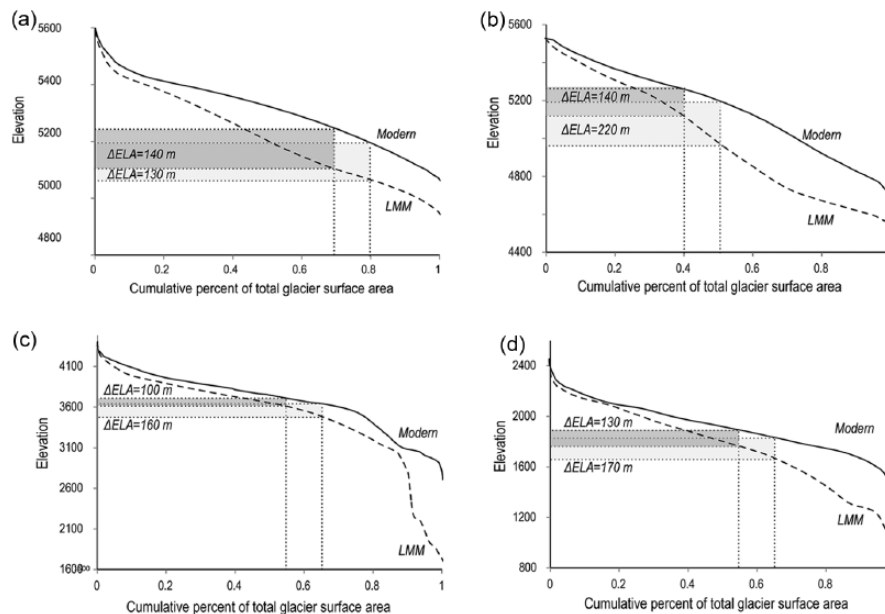
Climatic implications

Next, we consider the range of possible combination of temperature and precipitation anomalies required to change the ELA from the modern to LMM values (Figure 7).

Assuming that ELA changes are because of only temperature, at the Vilcanota site, the ELA change can be explained by a cooling of at least 0.7°C . Considering a change in precipitation only, the LMM ELA can be explained by an increase of more than 0.52 m yr^{-1} (representing a 64% of the present-day annual precipitation). At Cipreses and Tranquilo glaciers, the ELA changes can be explained by cooling of at least 0.6°C and 0.7°C or by precipitation increase of at least 0.22 (27%) and 0.30 m yr^{-1} (27%), respectively. Finally, at Tapado glacier, where the maximum ELA depression was observed, the ELA change can be explained by a temperature decrease of at least 1.0°C (assuming no changes in precipitation) or by a precipitation increase of more than 0.31 m yr^{-1} (89%, and no change in temperature). For the later site, negative anomalies of precipitation were not included because the SEMB model does not

Table 7. Modern and LLM equilibrium line altitudes. Values were calculated using different AAR values (see the ‘Methods’ section).

	Vilcanota		Tapado		Cipreses			Tranquilo	
AAR	0.7	0.8	0.4	0.5	0.55	0.65	0.55	0.66	
Modern ELA	5245	5195	5255	5195	3715	3645	1895	1835	
LMM ELA	5105	5065	5115	4975	3615	3485	1765	1665	
Delta ELA	140	130	140	220	100	160	130	170	

**Figure 6.** Hypsometry of the studied glacier. Solid lines represent modern hypsometry of the glaciers: (a) Cordillera Vilcanota, (b) Cerro Tapado, (c) Río Cipreses valley, and (d) Río Tranquilo valley. Dashed lines represent reconstructed hypsometry of the Last Millennium Maximum. Vertical dotted lines intersect the X axis in the AAR value selected for each site. Horizontal dotted lines intersect the Y axis in the corresponding ELA.

perform adequately when subjected to extremely low values of precipitation (Sagredo et al., 2014) (Figure 7).

Some of the changes in precipitation determined above could be considered unlikely. For example, at Tapado glacier, the change of precipitation required to decrease the ELA to its LMM elevation (without changing temperature) represents an increase in precipitation of 89%. For reference, Figure 7 (inset) shows the precipitation anomalies (m yr^{-1}) that represent a 25%, 50%, 75%, and 100% increase of annual values; in addition, we included the present-day temperature and precipitation interannual variability (± 1 standard deviation of the mean conditions for the period 1961–1990).

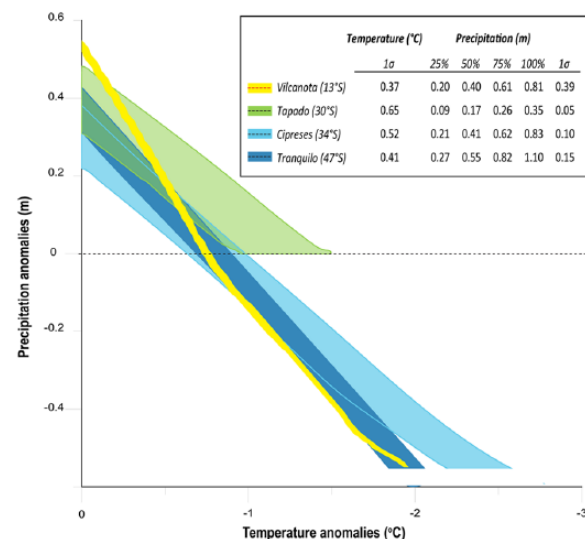
Overall, the model results show that the range of possible temperature and precipitation anomalies that accommodate the observed ELA changes at all four sites studied show minimum overlap. Conversely, this overlap is very high when comparing only the glaciers at Vilcanota, Cipreses, and Tranquilo sites. This implies that the climatic anomalies responsible for the drop in ELA at Tapado glacier are the most distinct.

Discussion

Next, we discuss our results derived from each of the steps involved in this research: timing of the LMM, ELA estimations, and climate reconstruction.

Chronology of the LMM

The chronology of the LMM relies on three different dating techniques, each of which has an analytical uncertainty (Tables 3, 5

**Figure 7.** Combination of temperature and precipitation anomalies (with respect to the present) that accommodate the ELA change from the Last Millennium Maximum to the present for the range of AARs used at each particular site. Color scheme is the same as in Figure 1. Inset: for reference, we included present-day temperature and precipitation variability (1σ) and values corresponding to 25%, 50%, 75%, and 100% of precipitation.

and 6). The relatively small number of dates available from the various geological contexts makes use of formal statistical tests impractical at the moment (Balco, 2011). Nevertheless, we

suggest that the post-depositional processes that may impact surface exposure ages (e.g. Applegate et al., 2012; Balco, 2011) are minimal because of the relatively short period of time that has passed since the LMM. Next, we contrast our dating results with prior studies where available.

On the northwest side of Cordillera Vilcanota, in the Upis-mayo valley, Mark et al. (2002) showed that the innermost moraine complex of the area was deposited after 340–560 cal yr BP (328 ± 46 ^{14}C yr BP). In addition, at Quelccaya Ice Cap (15 km to the southwest of Vilcanota site), Stroup et al. (2014, 2015) showed that the LMM in the Qori Kalis and Chalpacocha valley occurred at $>520 \pm 60$ yr BP. Similar results were obtained by Phillips et al. (2016), who constrained the LMM in the adjacent Huancané valley between 670 and 410 yr BP. These studies agree with our findings, supporting the idea that the LMM at the Vilcanota site occurred at <590 yr BP.

At Cipreses glacier, Röthlisberger (1987) radiocarbon dated two paleosols underlying lateral moraines in the upper portion of the valley (Figure 4c). The samples yielded ages of 5330–6610 cal yr BP (5180 ± 295 ^{14}C yr BP) and 360–860 cal yr BP (625 ± 155 ^{14}C yr BP), and represent maximum-limiting ages for the formation of the moraines. Unfortunately, these moraines are difficult to correlate with the aforementioned moraine complexes located downvalley, precluding comparison with the results of this study. Le Quesne et al. (2009) and Araneda et al. (2009) used historical records to infer that the Cipreses glacier margin was located near Medina II in CE 1842, implying that all the moraine complexes described above were deposited during the last ~170 years. Reexamining the evidence presented in these studies, we determined that the most conclusive record establishing the ice margin position comes from the description of Pissis' expedition to the area. Pissis (1875) determined that by 1858, the ice margin was located at an elevation of 1758 m a.s.l. This suggests that Cipreses glacier was near the Arriero moraines, and that Medina I and Medina II moraines were ice-free by the time of this observation. This hypothesis can be extrapolated to 1842, considering that Araneda et al. (2009) determined that by that time the ice was only 100 m downstream from the position identified by Pissis. Based on this, as well as our new dates, we suggest that the Medina I and Medina II moraines were deposited during the first half of the last millennium (between ~950 and 550 yr BP).

At Tranquilo glacier, we obtained three consistent ^{10}Be ages of ~5500 on the RT6 complex. These dates are statistically indistinguishable from the maximum age of 5280 ± 350 cal yr BP (4590 ± 115 ^{14}C yr BP) obtained by Mercer (1968) for a glacial advance in the eastern flank of the same massif ($47^{\circ}36'S$, $72^{\circ}14'W$).

Finally, the available dates suggest that while Tapado and Cipreses glaciers reached their LMM sometime during the first half of the last millennium, at Vilcanota this occurred at ~500 yr BP. We do not have chronological control over the LMM at Tranquilo glacier. Taken at face value, these preliminary data hint that the glaciers included in this study did not necessarily reach their LMM at the same time. However, we suggest that more chronological data are required to assess the synchrony (asynchrony) of these glacial events. For this reason, hereafter, we refer to the time when each glacier reached its maximum extent of the last 1000 years as the local LMM.

ELA estimates

ELA estimates for the study sites depend on reliable AAR values, which are known to vary from one climate regime to another. To overcome this problem, for each site we used a particular range of ELA values that are representative of each climate regime.

The results shown here suggest a significant overlap of the ELA changes across sites located in different climatic regimes along the Andes. Next, we compare our estimated ELA changes

with previous studies. Note that the exact timing of the glacial events compared here may vary from site to site, but all reflect the ELA depression during the most extensive advance of the last millennium.

At the Vilcanota site, the estimated ELA change since the local LMM is in good agreement with those calculated for neighboring areas. To the south, in the Cordillera Real, Bolivia (16°S , Figure 1), Rabatel et al. (2008) calculated an ELA change of ~150 m since the local LMM (~AD 1650), with a total range of 70–190 m. This result is very similar to our findings for the Vilcanota site (ΔELA 130–140 m). To the north, in Cordillera Blanca, Peru (Figure 1), Jomelli et al. (2008) proposed that glaciers reached similar maximum extents in CE 1350 and 1650. The ELA change between these maximum extents and the modern day was estimated to be ~180 m (Jomelli et al., 2008), somewhat larger than the findings presented here.

At the Cipreses glacier, our results also agree with previous studies within the same climate regime. At the El Peñón and El Azufre glaciers, in Central Argentina (35°S , Figure 1) (Espizua, 2005), the change in ELA since the local LMM was estimated to be 105 and 110 ± 50 m, respectively. These estimations fall within the range of ELA changes calculated for Cipreses glacier (100 to 160 m). No other studies have reported LMM ELAs for the climatic region of Tapado or Tranquilo glacier, precluding further comparisons. At least for the climate zones occupied by the Vilcanota site and Cipreses glacier, it can be argued that our estimates for ELA are compatible with other published results, which would suggest that our sites are capturing a regional signal rather than local anomalies.

Climate reconstruction

The ELA changes described above were used to reconstruct scenarios of climatic conditions during the LMM. We used the SEMB model to calculate the combination of temperature and precipitation anomalies that accommodate the ELA changes since the local LMM. The SEMB model was designed for application in large regions (Rupper and Roe, 2008). Factors such as the spatial resolution of the model inputs, the selection and application of constants in different areas, and the omission of topographic (e.g. hypsometry and slope) and glacio-dynamic effects in the calculation of the ELA increase model uncertainties when applied to smaller areas or single glaciers (Rupper and Roe, 2008). However, if it is assumed that the ELA change at each glacier site is representative of its climatic region, which is supported by a comparison of our data with previous studies, the SEMB model provides a first approximation of the range of climatic conditions during the local LMMs in the study areas. The results indicate that the range of possible temperature and precipitation anomalies overlap significantly at three of the four sites. This implies that if we assume that the LMM was synchronous across these three study areas (Vilcanota, Cipreses, and Tranquilo sites), it is possible that the climate anomalies responsible for the LMM were similar in the southern outer tropics, northernmost mid-latitudes, and Central Patagonia. It is unclear to us whether the climate anomalies reconstructed for Tapado glacier are distinct because (1) of a true spatial variability in the climate conditions during the LMM, (2) we are actually comparing non-contemporaneous glacial events, or (3) because of problems in the delimitation of former ice margins, which would impact local ELA reconstruction.

It has been shown that glaciers in the Andes exist under various climatic conditions, which control their responses to climate change. By combining a geomorphological reconstruction of glacial advances, dating of these glacial advances, and applying the same SEMB model to glaciers located in different climatic regimes, we provide new insights toward the understanding of the climatic conditions that influenced glacier extents at their

local LMMs along the Andes of South America. Our results fill information gaps and provide new data to understand Holocene climatic variability at a regional, hemispheric, and inter-hemispheric scale.

Summary and final remarks

- We reconstructed LHM climate conditions at four alpine glaciers located in different climate regimes along the Andes based on calculations of ELA changes and the application of a full SEMB model.
- The LMM occurred at ~500 yr BP at the Vilcanota site, and sometime during the first half of the last millennium at Tapado and Cipreses glaciers. We do not have chronological control for the LMM at Tranquilo glacier. The existing evidence is not sufficient to conclude that the LHM occurred synchronously across the study areas.
- There is a significant overlap in the ELA changes since the local LMM estimated for the four study areas (Vilcanota site: 130–140 m; Tapado glacier: 140–220 m; Cipreses glacier: 100–160 m; and Tranquilo glacier: 130–170 m).
- Assuming that the LMM was synchronous at Vilcanota, Cipreses, and Tranquilo sites, the SEMB model results suggest that it is possible that the climate anomalies responsible for the LMM were similar in the southern outer tropics, northernmost mid-latitudes, and Central Patagonia. It is unclear yet why Tapado glacier (in the subtropics) exhibits a distinct set of climate anomalies associated with the LMM.
- Our results contribute toward creating a broader network of climate proxy records, which can provide the foundations to test hypothesis regarding the mechanisms underlying the glacial events that occurred during the last millennium.

Acknowledgements

EA Sagredo acknowledges support from Fulbright-Conicyt Doctoral Fellowship and the Department of Geology at the University of Cincinnati. We thank Jennifer Howley for assistance in the cosmogenic nuclides laboratory at Dartmouth College. Our appreciation goes to Tomás Gómez, Jesús Soto, Justin Stroup, John Thompson, Samuel Beal, Yves, and Elena Cheiman, as well as the Crispín family for providing field assistance; and Fundación Altiplano MSV, Centro de Estudios Avanzados en Zonas Áridas (CEAZA), and Centro de Estudios del Cuaternario (CEQUA) for logistic support. We thank Brian H Luckman (UWO) and Colby A Smith for valuable discussion and insightful comments on the manuscript. Two anonymous reviewers provided constructive comments that improved the manuscript.

Funding

This work was funded by National Science Foundation Grants EAR-1003072, EAR-1003460; Fondecyt Iniciación 11121280; CONICYT USA2013-0035; and Iniciativa Científica Milenio NC120066.

References

- Applegate PJ, Urban NM, Keller K et al. (2012) Improved moraine age interpretations through explicit matching of geomorphic process models to cosmogenic nuclide measurements from single landforms. *Quaternary Research* 77: 293–304.
- Araneda A, Torrejón F, Aguayo M et al. (2009) Historical records of Cipreses glacier (34°S): Combining documentary-inferred ‘Little Ice Age’ evidence from Southern and Central Chile. *The Holocene* 19: 1173–1183.
- Aravena JC (2007) *Reconstructing climate variability using tree rings and glacier fluctuations in the southern Chilean Andes*. PhD Thesis, University of Western Ontario, 236 pp.
- Audebaud E (1973) Geología de los cuadrángulos de Ocongate y Sicuani: Hojas 28-t, 29-t. *Boletín del 25*.
- Bahr DB, Dyurgerov M and Meier MF (2009) Sea-level rise from glaciers and ice caps: A lower bound. *Geophysical Research Letters* 36: L03501.
- Balco G (2011) Contributions and unrealized potential contributions of cosmogenic-nuclide exposure dating to glacier chronology, 1990–2010. *Quaternary Science Reviews* 30: 3–27.
- Balco G, Stone JO, Lifton NA et al. (2008) A complete and easily accessible means of calculating surface exposure ages or erosion rates from ¹⁰Be and ²⁶Al measurements. *Quaternary Geochronology* 3: 174–195.
- Benn DI and Lehmkuhl F (2000) Mass balance and equilibrium-line altitudes on glaciers in high-mountain environments. *Quaternary International* 65–66: 15–29.
- Benn DI, Owen LA, Osmaston HA et al. (2005) Reconstruction of equilibrium-line altitudes for tropical and subtropical glaciers. *Quaternary International* 138–139: 8–21.
- Boninsegna J, Argollo J, Aravena J et al. (2009) Dendroclimatological reconstructions in South America: A review. *Palaeogeography, Palaeoclimatology, Palaeoecology* 281: 210–228.
- Bown F, Rivera A and Acuña C (2008) Recent glacier variations at the Aconcagua basin, central Chilean Andes. *Annals of Glaciology* 48: 43–48.
- Briner JP (2009) Moraine pebbles and boulders yield indistinguishable ¹⁰Be ages: A case study from Colorado, USA. *Quaternary Geochronology* 4: 299–305.
- Broecker WS (2000) Was a change in thermohaline circulation responsible for the Little Ice Age? *Proceedings of the National Academy of Sciences of the United States of America* 97: 1339–1342.
- Christie DA, Boninsegna JA, Cleaveland MK et al. (2011) Aridity changes in the Temperate-Mediterranean transition of the Andes since AD 1346 reconstructed from tree-rings. *Climate Dynamics* 36: 1505–1521.
- Cuffey K and Paterson W (2010) *The Physics of Glaciers*. San Diego, CA: Academic Press.
- De Martonne E (1934) The Andes of North-West Argentina. *The Geographical Journal* 84: 1–14.
- Denton GH and Karlén W (1973) Holocene climatic variations: Their pattern and possible cause. *Quaternary Research* 3: 155–205.
- Desilets D and Zreda M (2003) Spatial and temporal distribution of secondary cosmic-ray nucleon intensities and applications to in-situ cosmogenic dating. *Earth and Planetary Science Letters* 206: 21–42.
- Dirección Meteorológica de Chile (2001) *Climatología de Chile*. Santiago, Chile: Dirección Meteorológica de Chile.
- Dunai TJ (2001) Influence of secular variation of the magnetic field on production rates of in situ produced cosmogenic nuclides. *Earth and Planetary Science Letters* 193: 197–212.
- Dyurgerov MB and Meier MF (2000) Twentieth century climate change: Evidence from small glaciers. *Proceedings of the National Academy of Sciences of the United States of America* 97: 1406–1411.
- Espizua LE (2005) Holocene glacial chronology of Valenzuela Valley, Mendoza Andes, Argentina. *The Holocene* 15: 1079–1085.
- Falaschi D, Bravo C, Masiokas M et al. (2013) First glacier inventory and recent changes in glacier area in the Monte San Lorenzo region (47°S), southern Patagonian Andes, South America. *Arctic, Antarctic, and Alpine Research* 45: 19–28.
- Favier V, Wagnon P and Ribstein P (2004) Glaciers of the outer and inner tropics: A different behaviour but a common response to climatic forcing. *Geophysical Research Letters* 31: 1–5.

- Garreaud RD, Vuille M, Compagnucci R et al. (2009) Present-day South American climate. *Palaeogeography, Palaeoclimatology, Palaeoecology* 281: 180–195.
- Ginot P, Schwikowski M, Schotterer U et al. (2002) Potential for climate variability reconstruction from Andean glaciochemical records. *Annals of Glaciology* 35: 443–450.
- Grove JM (2004) *Little Ice Ages: Ancient and Modern*. London: Routledge.
- Hurley JV, Vuille M, Hardy DR et al. (2015) Cold air incursions, $\delta^{18}\text{O}$ variability, and monsoon dynamics associated with snow days at Quelccaya Ice Cap, Peru. *Journal of Geophysical Research: Atmospheres* 120: 7467–7487.
- Jomelli V, Favier V, Rabatel A et al. (2009) Fluctuations of glaciers in the tropical Andes over the last millennium and palaeoclimatic implications: A review. *Palaeogeography, Palaeoclimatology, Palaeoecology* 281: 269–282.
- Jomelli V, Grancher D, Brunstein D et al. (2008) Recalibration of the yellow Rhizocarpon growth curve in the Cordillera Blanca (Peru) and implications for LIA chronology. *Geomorphology* 93: 201–212.
- Kalnay E, Kanamitsu M, Kistler R et al. (1996) The NCEP/NCAR 40-year reanalysis project. *Bulletin of the American Meteorological Society* 77: 437–471.
- Kaplan MR, Strelin JA, Schaefer JM et al. (2011) In-situ cosmogenic ^{10}Be production rate at Lago Argentino, Patagonia: Implications for late-glacial climate chronology. *Earth and Planetary Science Letters* 309: 21–32.
- Kaser G (2001) Glacier-climate interaction at low latitudes. *Journal of Glaciology* 47: 195–204.
- Kaser G and Osmaston H (2002) *Tropical Glaciers*. Cambridge: Cambridge University Press.
- Kayastha RB, Ohata T and Ageta Y (1999) Application of a mass-balance model to a Himalayan glacier. *Journal of Glaciology* 45: 559–567.
- Kelly MA (2003) *The Late Würmian Age in the Western Swiss Alps – Last Glacial Maximum (LGM) Ice-Surface Reconstruction and ^{10}Be Dating of Late-Glacial Features*. Bern: University of Bern, 105 pp.
- Kelly MA, Lowell TV, Applegate PJ et al. (2015) A locally calibrated, late glacial ^{10}Be production rate from a low-latitude, high-altitude site in the Peruvian Andes. *Quaternary Geochronology* 26: 70–85.
- Kull C, Grosjean M and Veit H (2002) Modeling modern and late Pleistocene Glacio-climatological conditions in the North Chilean Andes (29–30° S). *Climatic Change* 52: 359–381.
- Lal D (1991) Cosmic ray labeling of erosion surfaces: In-situ nuclide production rates and erosion models. *Earth and Planetary Science Letters* 104: 424–439.
- Le Quesne C, Acuña C, Boninsegna JA et al. (2009) Long-term glacier variations in the Central Andes of Argentina and Chile, inferred from historical records and tree-ring reconstructed precipitation. *Palaeogeography, Palaeoclimatology, Palaeoecology* 281: 334–344.
- Leclercq PW, Oerlemans J, Basagic HJ et al. (2014) A data set of worldwide glacier length fluctuations. *The Cryosphere* 8: 659–672.
- Lifton N, Sato T and Dunai TJ (2014) Scaling in situ cosmogenic nuclide production rates using analytical approximations to atmospheric cosmic-ray fluxes. *Earth and Planetary Science Letters* 386: 149–160.
- Lifton N, Smart D and Shea M (2008) Scaling time-integrated in situ cosmogenic nuclide production rates using a continuous geomagnetic model. *Earth and Planetary Science Letters* 268: 190–201.
- Mann ME, Zhang Z, Rutherford S et al. (2009) Global signatures and dynamical origins of the Little Ice Age and medieval climate anomaly. *Science* 326: 1256.
- Marengo JA, Soares WR, Saulo C et al. (2004) Climatology of the low-level jet east of the Andes as derived from the NCEP-NCAR reanalyses: Characteristics and temporal variability. *Journal of Climate* 17: 2261–2280.
- Mark BG, Seltzer GO and Goodman AY (2002) Rates of deglaciation during the Last Glaciation and Holocene in the Cordillera Vilcanota-Queelccaya Ice Cap region, Southeastern Perú. *Quaternary Research* 57: 287–298.
- Marrero SM, Phillips FM, Borchers B et al. (2016) Cosmogenic nuclide systematics and the CRONUScal program. *Quaternary Geochronology* 31: 160–187.
- Masiokas MH, Rivera A, Espizua LE et al. (2009) Glacier fluctuations in extratropical South America during the past 1000 years. *Palaeogeography, Palaeoclimatology, Palaeoecology* 281: 242–268.
- Masiokas MH, Villalba R, Luckman BH et al. (2006) Snowpack variations in the central Andes of Argentina and Chile, 1951–2005: Large-scale atmospheric influences and implications for water resources in the region. *Journal of Climate* 19: 6334–6352.
- Meier MF and Post A (1962) Recent variations in mass net budgets of glaciers in western North America. *International Association of Hydrological Sciences Publication* 58: 63–77.
- Mercer JH (1968) Variations of some Patagonian glaciers since the Late-Glacial. *American Journal of Science* 266: 91–109.
- Mercer JH and Palacios O (1977) Radiocarbon dating of the last glaciation in Peru. *Geology* 5: 600–604.
- Miller GH, Geirsdóttir A, Zhong Y et al. (2012) Abrupt onset of the Little Ice Age triggered by volcanism and sustained by sea ice/ocean feedbacks. *Geophysical Research Letters* 39: L02708.
- Mölg T and Hardy DR (2004) Ablation and associated energy balance of a horizontal glacier surface on Kilimanjaro. *Journal of Geophysical Research: Atmospheres* 109: D16104.
- Morales M, Christie D, Villalba R et al. (2011) Precipitation changes in the South American Altiplano since 1300 AD reconstructed by tree-rings. *Climate of the Past Discussions* 7: 4297–4334.
- Moreno PI, Vilanova I, Villa-Martínez R et al. (2014) Southern Annular Mode-like changes in southwestern Patagonia at centennial timescales over the last three millennia. *Nature communications* 5: 4375.
- Moy CM, Moreno PI, Dunbar RB et al. (2009) Climate change in Southern South America during the last two millennia. In: Vimeux F (ed.) *Past Climate Variability in South America and Surrounding Regions, Developments in Paleoenvironmental Research*. Dordrecht: Springer, pp. 353–393.
- Neukom R, Luterbacher J, Villalba R et al. (2010) Multi-centennial summer and winter precipitation variability in southern South America. *Geophysical Research Letters* 37: L14708.
- Neukom R, Luterbacher J, Villalba R et al. (2011) Multiproxy summer and winter surface air temperature field reconstructions for southern South America covering the past centuries. *Climate Dynamics* 37: 35–51.
- New M, Lister D, Hulme M et al. (2002) A high-resolution data set of surface climate over global land areas. *Climate Research* 22: 1–25.
- Nishiizumi K, Imamura M, Caffee M et al. (2007) Absolute calibration of ^{10}Be AMS standards. *Nuclear Instruments and Methods in Physics Research B* 258: 403–413.
- Osborn TJ and Briffa KR (2006) The spatial extent of 20th-century warmth in the context of the past 1200 years. *Science* 311: 841–844.
- Pfeffer WT, Arendt AA, Bliss A et al. (2014) The Randolph Glacier Inventory: A globally complete inventory of glaciers. *Journal of Glaciology* 60: 537–552.
- Phillips FM, Kelly MA, Hudson AM et al. (2016) CRONUS-Earth calibration samples from the Huancané II moraines,

- Quelccaya Ice Cap, Peru. *Quaternary Geochronology* 31: 220–236.
- Pigati JS and Lifton NA (2004) Geomagnetic effects on time-integrated cosmogenic nuclide production with emphasis on in situ ^{14}C and ^{10}Be . *Earth and Planetary Science Letters* 226: 193–205.
- Pissis PA (1875) Excursión al cajon de los Cipreses en la hacienda de Cauquenes (Rancagua), por el doctor don Rodolfo A. Philippi. *Anales de la Universidad de Chile* 47: 651–670.
- Plummer MA and Phillips FM (2003) A 2-D numerical model of snow/ice energy balance and ice flow for paleoclimatic interpretation of glacial geomorphic features. *Quaternary Science Reviews* 22: 1389–1406.
- Porter SC (1975) Equilibrium line altitudes of late Quaternary glaciers in the Southern Alps, New Zealand. *Quaternary Research* 5: 27–47.
- Porter SC (2001) Snowline depression in the tropics during the last glaciation. *Quaternary Science Reviews* 20: 1067–1091.
- Porter SC and Denton GH (1967) Chronology of neoglaciation in the North American Cordillera. *American Journal of Science* 265: 177–210.
- Putnam AE, Schaefer JM, Barrell DJA et al. (2010) In situ cosmogenic ^{10}Be production-rate calibration from the Southern Alps, New Zealand. *Quaternary Geochronology* 5: 392–409.
- Rabatel A, Francou B, Jomelli V et al. (2008) A chronology of the Little Ice Age in the tropical Andes of Bolivia (16 S) and its implications for climate reconstruction. *Quaternary Research* 70: 198–212.
- Reid TD and Brock BW (2010) An energy-balance model for debris-covered glaciers including heat conduction through the debris layer. *Journal of Glaciology* 56: 903–916.
- Reimer PJ, Bard E, Bayliss A et al. (2013) IntCal13 and Marine13 radiocarbon age calibration curves 0–50,000 years cal BP. *Radiocarbon* 55: 1869–1887.
- Rodbell DT, Smith JA and Mark BG (2009) Glaciation in the Andes during the Lateglacial and Holocene. *Quaternary Science Reviews* 28: 2165–2212.
- Röthlisberger F (1987) *10000 Jahre Gletschergeschichte der Erde*. Aarau: Verlag Sauerlander.
- Rupper S and Roe G (2008) Glacier changes and regional climate: A mass and energy balance approach. *Journal of Climate* 21: 5384–5401.
- Sagredo E and Lowell T (2012) Climatology of Andean glaciers: A framework to understand glacier response to climate change. *Global and Planetary Change* 86–87: 101–109.
- Sagredo EA, Rupper S and Lowell TV (2014) Sensitivity of the equilibrium line altitude across the Andes. *Quaternary Research* 81: 355–366.
- Schotterer U, Grosjean M, Stichler W et al. (2003) Glaciers and climate in the Andes between the equator and 30°S: What is recorded under extreme environmental conditions? *Climatic Change* 59: 157–175.
- Seltzer GO (1994) Climatic interpretation of the alpine snowline variations on millennial time scales. *Quaternary Research* 41: 154–159.
- Senese A, Diolaiuti G, Mihalcea C et al. (2012) Energy and mass balance of Forni glacier (Stelvio National Park, Italian Alps) from a four-year meteorological data record. *Arctic, Antarctic, and Alpine Research* 44: 122–134.
- Solomina ON, Bradley RS, Jomelli V et al. (2016) Glacier fluctuations during the past 2000 years. *Quaternary Science Reviews* 149: 61–90.
- Stone JO (2000) Air pressure and cosmogenic isotope production. *Journal of Geophysical Research: Atmospheres* 105: 23753–23759.
- Stroup JS, Kelly MA, Lowell TV et al. (2014) Late-Holocene fluctuations of Qori Kalis outlet glacier, Quelccaya Ice Cap, Peruvian Andes. *Geology* 42: 347–350.
- Stroup JS, Kelly MA, Lowell TV et al. (2015) Late-Holocene fluctuations of Quelccaya Ice Cap, Peru, registered by nearby lake sediments. *Journal of Quaternary Science* 30: 830–840.
- Stuiver M and Reimer PJ (1993) Extended ^{14}C database and revised CALIB radiocarbon calibration program. *Radiocarbon* 35: 215–230.
- Villalba R (1994) Tree-ring and glacial evidence for the medieval warm epoch and the Little Ice Age in Southern South America. *Climatic Change* 26: 183–197.
- Vuille M and Ammann C (1997) Regional snowfall patterns in the high, arid Andes. *Climate Change* 36: 413–423.